

Trapping electrons in a room-temperature quadrupole trap

Clemens Matthiesen,^{1,*} Qian Yu,¹ Jinen Guo,¹ Alberto M. Alonso,¹ and Hartmut Häffner¹

¹*Department of Physics, University of California, Berkeley, California 94720, USA*

We demonstrate trapping of electrons in a millimeter-sized quadrupole Paul trap driven at 1.6 GHz in a room-temperature ultra-high vacuum setup. Cold electrons are introduced into the trap by ionization of atomic calcium via Rydberg states and stay confined by microwave and static electric fields for several tens of milliseconds. A fraction of these electrons remains trapped longer and shows no measurable loss for measurement times up to a second. Electronic excitation of the motion reveals secular frequencies from several tens to hundreds of MHz. Operating a similar electron Paul trap in a cryogenic environment may provide a platform for all-electric quantum computing with trapped electron spin qubits.

I. INTRODUCTION

The spin up and down states of an electron form the archetypal two-level system in quantum physics and make the electron a natural candidate for realizing a quantum bit. Quantum computing approaches use electrons in both condensed matter and atomic systems, for instance confined in quantum dots or bound to donors in semiconductors [1–3], or bound as valence electrons in trapped atomic ions [4, 5]. In these examples, the confinement to either the host solid-state environment or to a much heavier ion can limit the potential of the electron spin qubit: for trapped ions, entanglement is typically mediated by the slow motion of the heavy ions in a shared trapping potential [6, 7], which limits the gate speed, while in condensed matter systems unwanted coupling of the electron’s charge and magnetic moment to the imperfect environment limits coherence times.

An approach which promises to remove these limitations is to confine individual free electrons in actual vacuum [8–10]. Here we show experimentally that this can be achieved with the type of traps used for the currently most advanced ion trap quantum computers, namely quadrupole Paul traps. Compared to commonly trapped ions, the electron’s charge-to-mass ratio is larger by a factor $10^4 - 10^5$, such that motion-based gates and shuttling operations could be sped up by two orders of magnitude. Based on measurements for ion ground state qubits, which should experience similar decoherence mechanisms to trapped electron spin qubits, coherence times of at least a second are expected [11]. Furthermore, reducing the complex level structure down to the minimum of two levels rules out qubit errors due to population leakage [12]. Adapting the quantum-CCD architecture developed for trapped ions [13] to trapped electrons offers the opportunity to build a fast, modular, and high-fidelity quantum computer using advanced microwave technology [14–17], which promises better compatibility with current microfabrication methods compared to laser technology and optical beam delivery.

Beyond quantum computing, the experimental platform we introduce here may offer new avenues for creating and studying small cold plasma [18], highly controllable few- to single electron sources for electron optics applications [19], or single-electron mechanical oscillators [20].

Trapping single electrons in vacuum has previously been achieved in two other platforms. First electrons have been confined in cryogenic Penning traps in the early 1970s [21] by combining a large magnetic field and a constant electric quadrupole field. While several proposals have considered using single electrons in Penning traps as qubits [22–24], limited work has been performed on experimental realisations so far [25]. Electrons can also be trapped above the surface of liquid helium, offering quantum information applications in milli-Kelvin environments [26, 27] and recent experimental efforts have reached the single-electron regime [28].

Our approach to trapping electrons builds on the established quadrupole radiofrequency ion trap architecture, which is at the forefront of current quantum computing approaches with atomic ions [4, 5]. Guiding electrons along a radiofrequency guide [29] has been achieved and electrons have been co-trapped with ions in a combined Paul and Penning trap [30], but trapping electrons in a pure Paul trap has not been reported so far. While potential applications to quantum computing will require cryogenic environments [8–10], we concentrate here on demonstrating electron trapping in a proof-of-principle experiment at room temperature.

Paul traps employ a rapidly oscillating quadrupole electric field to confine charged particles at the null of the quadrupole field in two or three dimensions. The effective confining potential can be described by the pseudopotential $U_p = \frac{q^2 E^2}{4m\Omega^2}$, where E and Ω are the amplitude and frequency of the oscillating electric field, and q and m the charge and mass of the trapped particle(s). The spatial dependence $U_p(x, y, z)$ derives from the quadrupole electric field amplitude $E(x, y, z)$. The stability of trajectories for a charged particle in a quadrupole trap can be described with the a and q parameters of the Mathieu equation, which are known as the stability parameters in the context of ion traps, and have been studied theoretically and experimentally [31, 32]. Typically, trajectories

* Corresponding author: cm467@berkeley.edu

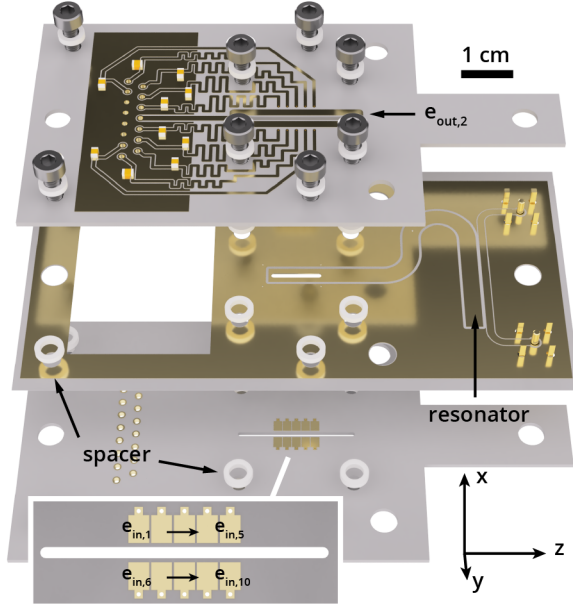


FIG. 1. Electron trap design. Exploded view of trap printed circuit boards. Driving the halfwave co-planar waveguide resonator (central board) gives rise to a quadrupole microwave trap inside the slot at the central end of the resonator. The two outside boards are identical and feature electrodes $e_{in,1-10}$ ($e_{in,11-20}$) on the bottom (top) to provide static confinement along the slot direction (see bottom inset for electrode labels). The boards are separated with alumina spacers of 1.27 mm height and have a footprint of about 5 by 10 cm.

in the trap are stable if the frequency of motion ω of the particles in the potential is much slower than the frequency Ω of the confining field, and if the pseudopotential depth, defined as the maximum of the pseudopotential, is much larger than the kinetic energy of the charged particles.

There are three main challenges to moving from ion to electron trapping: first, due to the lower electron mass the trapping field must be at higher frequencies. The stability parameters (a and q) and depth of a quadrupole trap scale as $(m\Omega^2)^{-1}$, requiring the drive frequency Ω for an electron trap to be about two orders of magnitude higher than for typical ion traps. Second, electrons must be created with energies low enough to stay confined by the trapping potential. We require both that cold electrons are injected directly into the trap center, and that the trap is sufficiently deep. Third, in the absence of fluorescence detection, we need a different mechanism to evidence trapping.

II. EXPERIMENT DESIGN

A. Electron trap

We begin by describing the microwave quadrupole trap engineered for this experiment, shown in an exploded view in Fig. 1. It consists of three double-sided printed circuit boards (PCBs) separated by alumina spacers. The central board features a co-planar $\lambda/2$ waveguide resonator capacitively coupled to a microwave feedline (right-hand side of the PCB). The end of the resonator in the board center contains a slot and functions as the trap's microwave electrode, providing an AC quadrupole field which confines electrons inside the slot in the x and y -directions. The quality factor of the resonator is about 35. When fully assembled and connected inside the ultra-high vacuum (UHV) chamber, we measure a resonance frequency of $2\pi \times 1.60$ GHz, and find we can reach about 100 V on the microwave resonator with 5 W input power. Integrating a co-planar resonator into the trap design provides a convenient solution to reaching the high frequencies needed for electron trapping and future cryogenic experiments can take advantage of previous work on waveguide resonators in the context of superconducting qubits [33, 34]. The resonator is held at DC ground potential via a tap in its center which connects it to the grounded top surface of the board. The outside PCBs, mirroring each other about the central board, each feature ten rectangular electrodes along the slot on the inside board surface, labeled $e_{in,j}$ with $j = 1 - 20$. Electrodes $e_{in,1-10}$ are visible on the lower board and magnified in the inset, while electrodes $e_{in,11-20}$ are on the hidden side of the upper board. The traces delivering voltages to the electrodes are on the outside surfaces, visible for the top board, and linked to a ground electrode via 10 pF decoupling capacitors. Both boards also feature a single electrode which surrounds the slot on the outside surface, and is labeled $e_{out,1}$ for the bottom board and $e_{out,2}$ for the top board. Electrodes $e_{in,1-20}$ are used to apply a static quadrupole field, confining electrons in the z (axial) direction, while $e_{out,1-2}$ are held at DC ground potential. Wires soldered to the outer boards supply DC voltages in the ± 28 V range from a 16 bit digital-to-analog-converter, while the microwave voltage is applied via SMA connectors to the central board.

Fig. 2 details the trap pseudopotential experienced by an electron when the resonator supplies 90 V at $2\pi \times 1.6$ GHz and all DC electrodes are grounded. Fig. 2(a) displays a map of the pseudopotential for a cut through the trap in the xy -plane at the center of the slot, highlighting the trap substrate and electrodes as hashed grey and yellow areas, respectively. In Fig. 2(b) and (c) we show that the trap depth based on the pseudopotential approximation (continuous blue curves) is about 1.3 eV (or 15,000 K), limited by the weaker confinement along the x -direction. We compare the pseudopotential to an ideal harmonic potential (orange dashed curve) and find they match closely to a distance of about

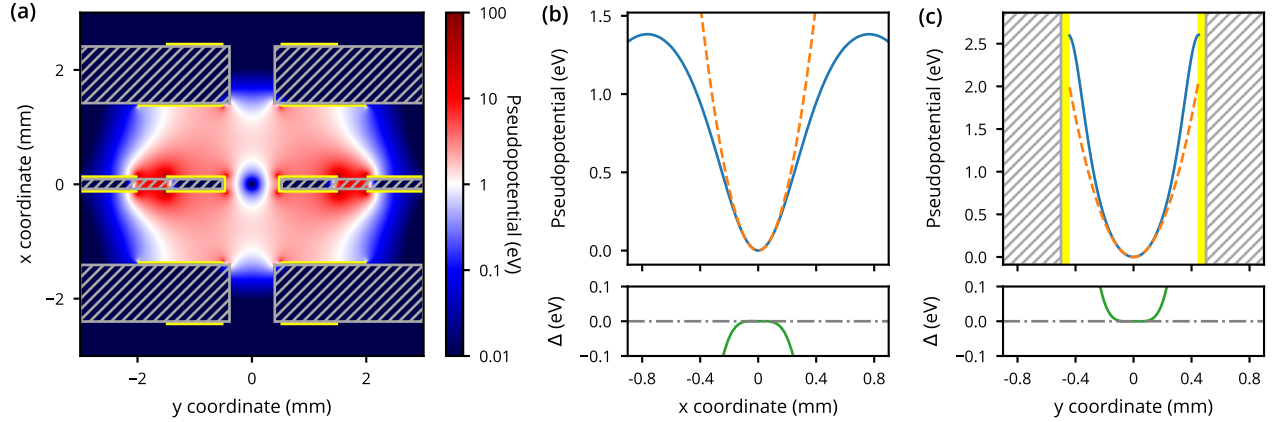


FIG. 2. Electron trapping potential. (a) Contour plot of the trapping potential based on the pseudopotential approximation in the xy -plane in the center of the slot for 90 V amplitude at 1.6 GHz frequency on the resonator electrode. The circuit board substrate is indicated by the hashed areas, metal electrodes are highlighted in yellow. (b) Top: pseudopotential along the x -axis through the trap center (blue continuous curve), compared to an ideal harmonic potential (dashed orange). Bottom: deviation Δ of pseudopotential from harmonic potential. (c) Top: pseudopotential along the y -axis through the trap center (blue continuous curve), compared to an ideal harmonic potential (dashed orange). Location of trap substrate (electrodes) shown as hashed grey (solid yellow) area. Bottom: deviation Δ of pseudopotential from harmonic potential.

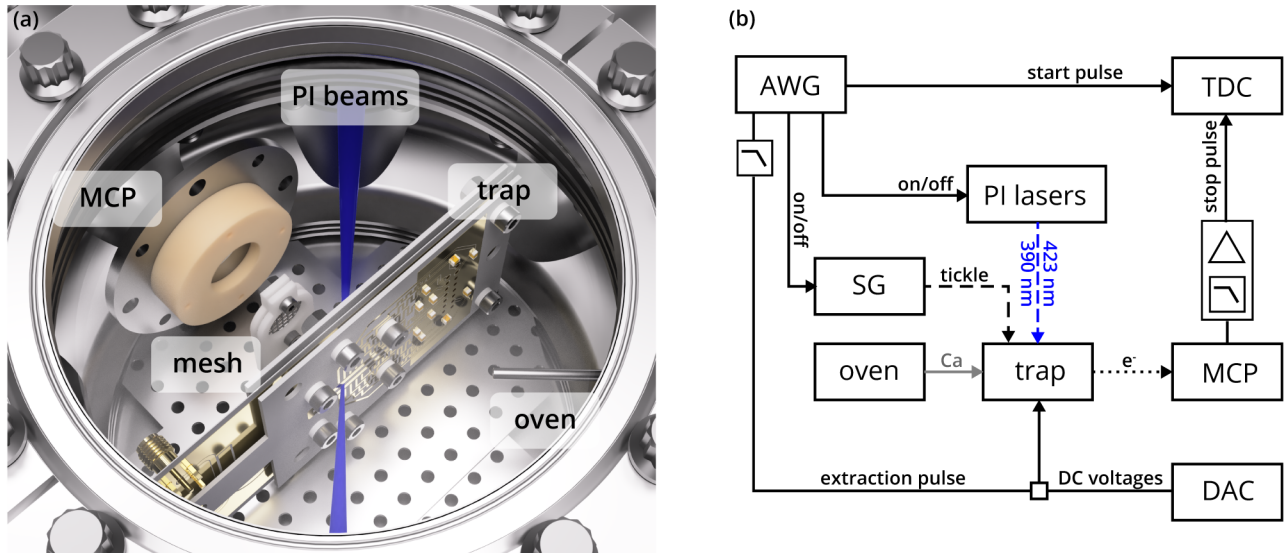


FIG. 3. Experimental setup and control schematic. (a) Simplified rendering of the setup inside the UHV chamber, showing the electron trap, a microchannel plate (MCP) detector, a mesh, the path of the PI beams, and an oven supplying calcium for ionization. (b) Key elements for experiment synchronization. An arbitrary waveform generator (AWG) provides the extraction pulses to the trap, and the start signal for a time-to-digital converter (TDC). It controls the timing for pulsing on and off the PI loading beams and a signal generator (SG), which excites the electron motion ('tickle'). Pulses from the MCP provide the stop Signals to the TDC. Low-pass filters prevent electronic pickup of the microwave trap drive and the extraction pulses by the MCP detection circuit which contains pulse shaping and amplification elements. The Ca oven and a digital-to-analog converter (DAC) for the DC trap voltages are operated with constant settings during an experiment.

100 μ m from the trap center, as exemplified by the green curves in the bottom panels which show their difference Δ . The secular frequency for an electron moving in this potential (radial modes of motion) corresponds to about $2\pi \times 300$ MHz.

B. Electron loading and detection

With a suitable trap design in place, we address the challenges of injecting electrons into the trap and detecting them. Previous experiments involving trapping electrons in Penning traps, or guiding electrons in a

linear quadrupole potential employed electron guns, either as primary electron source [29], or to create secondary electrons through collision ionization of background gas [30, 35]. Here, we borrow the two-stage procedure for photoionization (PI) of calcium which is used for trapping ions from an atomic beam [36]. It enables both the creation of very cold electrons by tuning the lasers close to the ionization threshold, and preferential ionization in the trapping region by optical alignment. Since fewer charged particles are introduced around the trap using this method, we also reduce accidental charging of the trap which would modify the trapping potential. Detection is accomplished by applying voltage pulses to several DC electrodes which distort the trapping potential to extract trapped electrons, and accelerate them into a microchannel plate detector (MCP).

C. Experiment setup and protocol

The main components of the experimental setup and their alignment in the UHV chamber are shown in Fig. 3(a), omitting electric leads for simplicity. The base pressure in the chamber is below 1×10^{-10} mbar. In addition to the trap itself, the chamber contains a resistive oven aligned to direct an atomic calcium beam through the trap slots when heated (steel tube labelled ‘oven’), the two-stage MCP, and a steel mesh which directs electrons extracted from the trap towards the MCP. The photoionization laser beams (423 and 390 nm wavelength) are overlapped and traverse the chamber at right angles to the Ca oven, focusing near the trapping region with a beam waist of about 30 μm . The 423 nm single-mode laser is tuned to be on resonance with the neutral calcium 4^1S_0 - 4^1P_1 transition, while the free-running multi-mode 390 nm laser diode is tuned by temperature and current to maximise the electron ionization rate. While the 4^1P_1 -continuum ionization threshold is at about 389.8 nm, we find the ionization rate to peak when the diode center wavelength is about 390.3 ± 0.2 nm, suggesting ionization is taking place via Rydberg states [36]. As such, we expect electrons to inherit only minimal kinetic energy from the ionization process and their energy in the trapping potential is rather determined by their ionization location.

Fig. 3(b) shows a schematic of the electronics setup for synchronizing the experiment. An arbitrary waveform generator (AWG) functions as the experiment clock, providing the trap extraction pulse, and the start signal triggering a time-to-digital-converter (TDC). The extraction pulses are added to the static voltages for DC confinement which originate from a digital-to-analog converter (DAC). The AWG further controls the timing for switching on and off both the 390-nm PI laser for loading and a signal generator (SG) used to apply an rf tone (labeled ‘tickle’) to the trap. The electron detection signal is picked off from the MCP anode supply voltage with a high-pass filter, shaped and amplified it so that it can

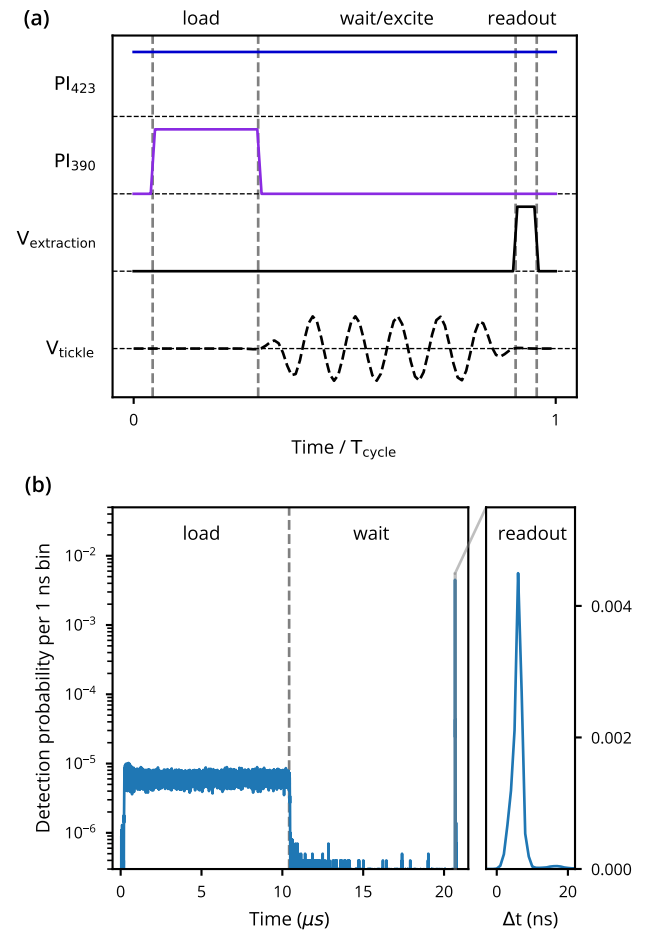


FIG. 4. Measurement protocol and typical data. (a) Illustration of one cycle of the experimental protocol. Free electrons are created during the loading phase when the 390-nm laser is switched on. An rf tone is applied to one DC electrode in some experiments during the ‘wait/excite’ phase. Voltage pulses to three DC electrodes in the ‘readout’ phase eject electrons in the direction of the mesh and MCP. (b) Histogram of MCP detection events for experiment with load and wait times $t_{\text{load}} = t_{\text{wait}} \approx 10 \mu\text{s}$. During loading, some untrapped electrons are accelerated into the MCP, replicating the 390 nm laser pulse shape. The extraction pulse empties the trap into the MCP, resulting in a large and sharply localized signal. Inset: Close-up of the histogram during the readout phase.

be used as the TDC stop signal. Low-pass filtering the extraction pulses ($2\pi \times 50$ MHz cut-off) prevents electronic pickup at the MCP and a further low-pass filter ($2\pi \times 200$ MHz cut-off) in front of the shaping and amplification circuit removes pickup at the frequency of the microwave drive.

The timing for one experimental cycle is illustrated in Fig. 4(a). It starts with a loading phase of variable length t_{load} where the 390 nm PI laser is pulsed on. The 423 nm PI laser is kept on during the full cycle. Loading is followed by a variable time t_{wait} , where we either keep all settings constant or apply an rf tone at frequency

ω_{tickle} to electrode $e_{\text{in},17}$. Finally, an extraction pulse of 20 ns duration is applied to three electrodes, $e_{\text{out},1}$ with 14 V amplitude, and $e_{\text{in},3,8}$ with 10 V amplitude, which ejects trapped charges from the trap. For the experiments presented here we supply a constant current to the calcium oven, and keep the microwave trap drive in continuous-wave mode such that the voltage amplitude on the microwave resonator corresponds to about 90 V. 500 μW of 423 nm laser light and approximately 2.4 mW of 390 nm light are sent through the chamber. The mesh is at 150 V potential while the first and second stage, and the anode of the MCP are kept at 200 V, 2200 V and 2500 V, respectively.

In Fig. 4(b) we show a histogram of MCP detection events, where the loading and wait times are $t_{\text{load}} = t_{\text{wait}} \approx 10 \mu\text{s}$. Data are displayed as probability to record an event during a 1 ns time bin and we acquire data for 10^7 experimental cycles. During the loading period we observe a small constant signal mirroring the shape of the 390 nm laser pulse, likely from just created but not trapped electrons. Application of the extraction pulse at the end of the experimental cycle results in a large and sharply localized signal from the MCP, demonstrating that electrons remain in the trap 10 μs after the end of the loading pulse. The inset displays a close-up of the readout signal, which peaks with a full-width at half-maximum of about 2 ns. Note the inset uses a linear scale for the readout signal, while the full cycle is displayed using a semi-logarithmic scale to show the background during loading as well.

III. RESULTS

A. Electron loading and storage

Having demonstrated electron trapping, we move on to quantify the trapping process. To investigate electron loading we use the protocol introduced in Fig. 4(a) and vary t_{load} for a fixed wait time $t_{\text{wait}} = 10 \mu\text{s}$. For ease of presentation, we sum detections over a 50-ns wide window around the readout signal, see Fig. 5(a) for the results. The left ordinate displays the fraction of cycles with at least one detection pulse from the MCP which approaches unity with a time constant $\tau_{1/e} \approx 80 \mu\text{s}$ as t_{load} increases. We employ a simple threshold method to detect MCP pulses with the TDC and set a 60 ns dead-time following each detection to prevent double counting some events due to voltage ringing, which sets a natural limit of one detection event per cycle. Considering the non-unity open area of both the mesh (0.5) and the MCP (0.6) as dominant loss sources we estimate about one third of extracted electrons result in a signal from the MCP. Taking into account the loss and the number of detections per cycle, we can estimate the average number of electrons in the trap for each measurement setting. The right ordinate in Fig. 5(a) shows that it takes on average 25 μs to load one electron and we trap on average

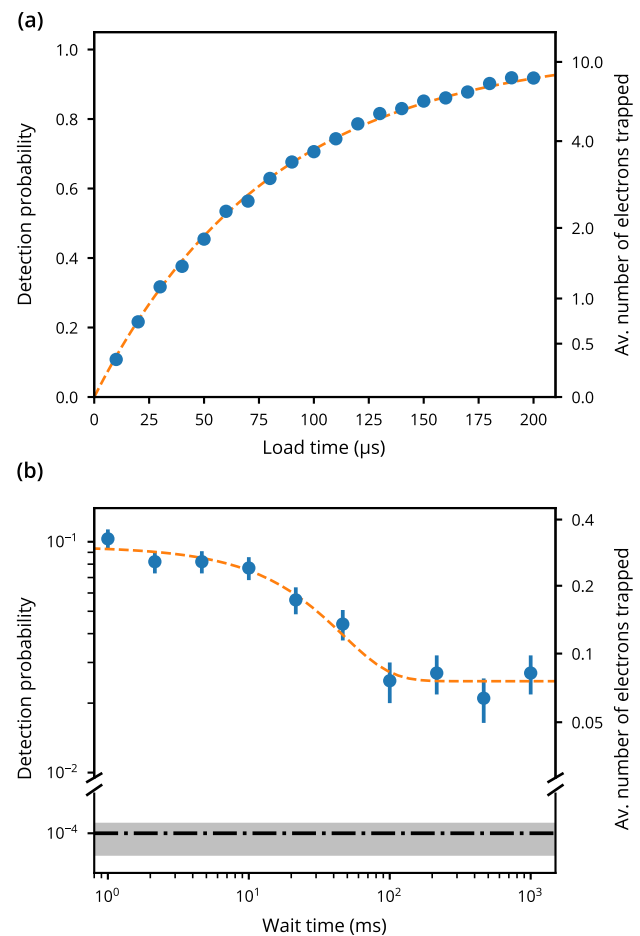


FIG. 5. Trapped electron loading and storage. (a) Electron trapping and detection probability as function of loading time with $t_{\text{wait}} = 10 \mu\text{s}$. The dashed curve shows an exponential fit to $1 - \exp(t/\tau_{1/e})$ with $\tau_{1/e} = 80.3 \pm 0.5 \mu\text{s}$. Error bars due to statistical uncertainty are too small to be visible. (b) Storage time measurement with a double-exponential fit, showing three quarters of electrons leave the trap with a decay constant $\tau_{1/e} = 30 \pm 7 \text{ ms}$, while the remaining quarter show no decay within measurement uncertainty. The horizontal dash-dotted line displays the background detection level based on an independent measurement. Error bars and the grey band correspond to one s. d. statistical uncertainty.

about 8 electrons for a loading time of 200 μs .

To measure the electron storage time in the trap, we set the loading time such that the trap rarely contains more than a single electron, and record the readout signal as function of the wait time, see Fig. 5(b) for the data. The measurement shows two distinct regimes, where about three quarters of electrons are lost within 100 ms (exponential decay with $\tau_{1/e} = 30 \pm 7 \text{ ms}$ for this measurement), while the remaining one quarter show no detectable loss after 1 s. The horizontal dash-dotted line displays the background detection level measured independently to be about 1×10^{-4} detections per cycle.

Any electron loss may seem surprising when just con-

sidering the pseudopotential trap depth since the electron energy due to the ionization process should be very small. Even fast thermalisation with the room-temperature environment would not provide enough energy to escape the trap. We have confirmed collisions with background gas are not the dominant loss mechanism by conducting measurements with different pressures in the chamber. Numerical simulations of electron trajectories in the time-dependent electric field from the microwave electrode suggest that electrons ionized at a distance of more than $120\ \mu\text{m}$ from the trap center are trapped initially, but eventually escape. This length scale is consistent with the extent of the strictly harmonic part of the trapping potential (cf. Fig. 2), pointing to the importance of trap harmonicity for particle storage [37]. We can qualitatively confirm this reasoning by changing the focusing and alignment of the PI beams, which affects the average ionization distance from the trap center, and find larger PI beams in the trapping region are correlated with fewer long-lived electrons.

We also observe the initial electron loss to only accelerate very slightly when we increase the number of trapped charges, indicating only weak interaction between the few charges in the trap. Studying the loss mechanisms of trapped electrons in greater detail with this Paul trap will likely be an important subject for future work. However, the long lifetimes observed here show that heating effects, for instance due to collisions with background gas or the electron micromotion (rf heating) [38] are not prohibitive to conducting experiments even at room temperature. This is an encouraging sign, in particular for the prospects of non-destructive electron detection and cooling via image current measurements in a cryogenic environment. Studying trap loss may also yield insights relevant for quadrupole ion traps, and since the electron motion is faster by a factor of a hundred compared to ion motion in typical trap, experiments would take less time.

B. Trap frequencies

Finally we are interested in the frequencies of the electron motion in the trap. Again, we follow the experimental protocol from Fig. 4(a), now loading about four electrons on average, and setting the wait time to $t_{\text{wait}} = 2\ \text{ms}$. During the wait time we try to excite the motion of trapped electrons with an rf tone at frequency ω_{tickle} . We step ω_{tickle} in increments of 1 MHz from 20 to 350 MHz and monitor electron loss, which is indicative of a motional resonance. The top panel in Fig. 6 shows the electron loss spectrum for a tickle voltage of about 5 mV applied to e_{in} ,¹⁷ and features two prominent dips. We can identify the resonances based on their response to DC and microwave voltages, revealing the dip at about $2\pi \times 40\ \text{MHz}$ as the axial mode, while the $2\pi \times 300\ \text{MHz}$ resonance is due to one of the radial modes of motion. We find no evidence of multi-electron Wigner crystal modes, which is consistent with having weakly or non-interacting

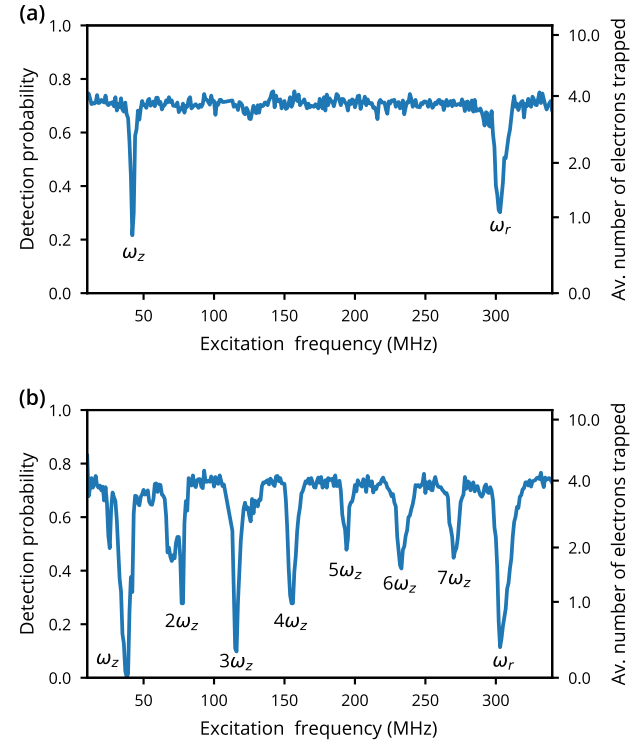


FIG. 6. Trap frequencies. Measurements of the motional resonances for an average of four electrons loaded into the trap, and a wait time $t_{\text{wait}} = 2\ \text{ms}$ during which an rf tickle is switched on. The axial (radial) resonance is denoted ω_z (ω_r). (a) 5 mV tickle excitation, (b) 20 mV tickle excitation.

electrons with a range of energies in the trap.

For low excitation tickle powers only the fundamental resonances are visible. Exciting the system more strongly reveals a series of harmonics of the axial mode (see Fig. 6(b)), and a small shift in the fundamental frequency. Changing the DC and microwave voltages, we can tune the axial mode frequency between 30 and 100 MHz and the radial mode between 200 and 380 MHz, limited by the voltage sources used in the experiment.

IV. CONCLUSIONS

In summary, we have presented the first experiment to trap single to few electrons in a microwave Paul trap. Electrons can be loaded in several tens of microseconds and 25% survive up to at least one second. Trap frequencies ranging from several 10 MHz to several 100 MHz have been demonstrated.

Trapping electrons in a Paul trap opens the door to using their unique properties for quantum information processing. The next milestones towards this goal will be to bring motional frequencies into the GHz regime with smaller traps, and integrate them into a cryogenic environment, which should enable non-destructive elec-

tron detection [21] and spin readout [9]. Building on technology that has already been demonstrated for quantum control of trapped ion hyperfine [14–17] and Zeeman [11] qubits could accelerate the development of a trapped electron quantum computing platform. While distribution of entanglement over large distances appears challenging, dipole-dipole coupling of single electrons, or electron crystals, in separate traps is an attractive alternative to realizing entanglement over intermediate distances [39, 40]. Another path towards coupling electron qubits over longer distances could be via image currents in shared electrodes [41, 42]. Techniques like these may enable creation of large entangled states.

We also note that an electron in the harmonic potential of a Paul trap realizes an instance of the lightest possible electromechanical oscillator [43]. The resonance frequency and quality factor can be engineered by controlling the confining potential. The ability to fine-tune the frequency of motion *in-situ* and the electron’s strong interaction with electric fields could be used for coupling

to other quantum systems with resonances in the GHz range, such as superconducting qubits [10, 44]. Electron Paul traps may also find applications outside the realm of quantum information science. Our trap could, for instance, trap positrons and be employed for the preparation of antihydrogen [45, 46]. Other applications include electric-field sensing at GHz frequencies [47], using cold trapped electrons for imaging [19], or for plasma physics studies [18].

ACKNOWLEDGMENTS

We would like to thank S. Mouradian for manuscript feedback, the Yao lab at UC Berkeley for loan of the TDC, and Dr David E. Root, Keysight Laboratories, for initiating financial support and technical assistance by Keysight Technologies through the Keysight University Research Collaborations Program.

-
- [1] T. F. Watson, S. G. Philips, E. Kawakami, D. R. Ward, P. Scarlino, M. Veldhorst, D. E. Savage, M. G. Lagally, M. Friesen, S. N. Coppersmith, M. A. Eriksson, and L. M. Vandersypen, A programmable two-qubit quantum processor in silicon, *Nature* **555**, 633 (2018).
- [2] J. Yoneda, K. Takeda, T. Otsuka, T. Nakajima, M. R. Delbecq, G. Allison, T. Honda, T. Kodera, S. Oda, Y. Hoshi, N. Usami, K. M. Itoh, and S. Tarucha, A quantum-dot spin qubit with coherence limited by charge noise and fidelity higher than 99.9%, *Nature Nanotechnology* **13**, 102 (2018).
- [3] A. Laucht, R. Kalra, S. Simmons, J. P. Dehollain, J. T. Muhonen, F. A. Mohiyaddin, S. Freer, F. E. Hudson, K. M. Itoh, D. N. Jamieson, J. C. McCallum, A. S. Dzurak, and A. Morello, A dressed spin qubit in silicon, *Nature Nanotechnology* **12**, 61 (2017).
- [4] K. R. Brown, J. Kim, and C. Monroe, Co-designing a scalable quantum computer with trapped atomic ions, *npj Quantum Information* **2**, 1 (2016).
- [5] C. D. Bruzewicz, J. Chiaverini, R. McConnell, and J. M. Sage, Trapped-ion quantum computing: Progress and challenges, *Applied Physics Reviews* **6**, 10163/1.5088164 (2019).
- [6] A. S. Sørensen and K. Mølmer, Quantum Computation with Ions in Thermal Motion, *Physical Review Letters* **82**, 1971 (1999).
- [7] D. Leibfried, B. DeMarco, V. Meyer, D. Lucas, M. Barrett, J. Britton, W. M. Itano, B. Jelenković, C. Langer, T. Rosenband, and D. J. Wineland, Experimental demonstration of a robust, high-fidelity geometric two ion-qubit phase gate, *Nature* **422**, 412 (2003).
- [8] N. Daniilidis, D. J. Gorman, L. Tian, and H. Hartmut, Quantum information processing with trapped electrons and superconducting electronics, *New J. Phys.* **15**, 073017 (2013).
- [9] P. Peng, C. Matthiesen, and H. Häffner, Spin readout of trapped electron qubits, *Physical Review A* **95**, 012312 (2017).
- [10] S. Kotler, R. W. Simmonds, D. Leibfried, and D. J. Wineland, Hybrid quantum systems with trapped charged particles, *Physical Review A* **95**, 022327 (2017).
- [11] T. Ruster, C. T. Schmiegelow, H. Kaufmann, C. Warschburger, F. Schmidt-Kaler, and U. G. Poschinger, A long-lived Zeeman trapped-ion qubit, *Applied Physics B* **122**, 254 (2016).
- [12] N. C. Brown and K. R. Brown, Comparing Zeeman qubits to hyperfine qubits in the context of the surface code: Yb + 174 and Yb + 171, *Physical Review A* **97**, 052301 (2018).
- [13] D. Kielpinski, C. Monroe, and D. J. Wineland, Architecture for a large-scale ion-trap quantum computer., *Nature* **417**, 709 (2002).
- [14] F. Mintert and C. Wunderlich, Ion-Trap Quantum Logic Using Long-Wavelength Radiation, *Physical Review Letters* **87**, 257904 (2001).
- [15] C. Piltz, T. Sriarunothai, S. S. Ivanov, S. Wölk, and C. Wunderlich, Versatile microwave-driven trapped ion spin system for quantum information processing, *Science Advances* **2**, 1 (2016).
- [16] C. Ospelkaus, U. Warring, Y. Colombe, K. R. Brown, J. M. Amini, D. Leibfried, and D. J. Wineland, Microwave quantum logic gates for trapped ions, *Nature* **476**, 181 (2011).
- [17] T. P. Harty, M. A. Sepiol, D. T. C. Allcock, C. J. Ballance, J. E. Tarlton, and D. M. Lucas, High-Fidelity Trapped-Ion Quantum Logic Using Near-Field Microwaves, *Physical Review Letters* **117**, 140501 (2016).
- [18] K. A. Twedt and S. L. Rolston, Electronic detection of collective modes of an ultracold plasma, *Physical Review Letters* **108**, 065003 (2012).
- [19] P. Kruit, R. G. Hobbs, C. S. Kim, Y. Yang, V. R. Manfrinato, J. Hammer, S. Thomas, P. Weber, B. Klopfer, C. Kohstall, T. Juffmann, M. A. Kasevich, P. Hommelhoff, and K. K. Berggren, Designs for a quantum electron microscope, *Ultramicroscopy* **164**, 31 (2016).
- [20] S. C. Burd, R. Srinivas, J. J. Bollinger, A. C. Wilson,

- D. J. Wineland, D. Leibfried, D. H. Slichter, and D. T. Allcock, Quantum amplification of mechanical oscillator motion, *Science* **364**, 1163 (2019).
- [21] D. J. Wineland, P. Ekstrom, and H. Dehmelt, Monoelectron Oscillator, *Physical Review Letters* **31**, 1279 (1973).
- [22] G. Ciaramicoli, I. Marzoli, and P. Tombesi, Scalable Quantum Processor with Trapped Electrons, *Phys. Rev. Lett.* **91**, 17901 (2003).
- [23] I. Marzoli, P. Tombesi, G. Ciaramicoli, G. Werth, P. Bushev, S. Stahl, F. Schmidt-Kaler, M. Hellwig, C. Henkel, G. Marx, I. Jex, E. Stachowska, G. Szawiola, and A. Walaszyk, Experimental and theoretical challenges for the trapped electron quantum computer, *J. Phys. B: At. Mol. Opt. Phys* **42**, 154010 (2009).
- [24] J. Goldman and G. Gabrielse, Optimized planar Penning traps for quantum-information studies, *Physical Review A* **81**, 052335 (2010).
- [25] P. Bushev, S. Stahl, R. Natali, G. Marx, E. Stachowska, G. Werth, M. Hellwig, and F. Schmidt-Kaler, Electrons in a cryogenic planar Penning trap and experimental challenges for quantum processing, *The European Physical Journal D* **50**, 97 (2008).
- [26] S. A. Lyon, Spin-based quantum computing using electrons on liquid helium, *Physical Review A* **74**, 052338 (2006).
- [27] D. I. Schuster, A. Fragner, M. I. Dykman, S. A. Lyon, and R. J. Schoelkopf, Proposal for Manipulating and Detecting Spin and Orbital States of Trapped Electrons on Helium Using Cavity Quantum Electrodynamics, *Physical Review Letters* **105**, 40503 (2010).
- [28] G. Koolstra, G. Yang, and D. I. Schuster, Coupling a single electron on superfluid helium to a superconducting resonator, *Nature Communications* **10**, 5323 (2019).
- [29] J. Hoffrogge, R. Fröhlich, M. A. Kasevich, and P. Hommelhoff, Microwave Guiding of Electrons on a Chip, *Physical Review Letters* **106**, 193001 (2011).
- [30] J. Walz, S. B. Ross, C. Zimmermann, L. Ricci, M. Prevedelli, and T. W. Hansch, Combined Trap with the Potential for Antihydrogen Production, *Phys Rev Lett* **75**, 3257 (1995).
- [31] R. Alheit, X. Z. Chu, M. Hoefer, M. Holzki, G. Werth, and R. Blumel, Nonlinear collective oscillations of an ion cloud in a Paul trap, *Physical Review A* **56**, 4023 (1997).
- [32] D. Leibfried, R. Blatt, C. Monroe, and D. Wineland, Quantum dynamics of single trapped ions, *Reviews of Modern Physics* **75**, 281 (2003).
- [33] M. Goeppel, A. Fragner, M. Baur, R. Bianchetti, S. Filipp, J. M. Fink, P. J. Leek, G. Puebla, L. Steffen, and A. Wallraff, Coplanar waveguide resonators for circuit quantum electrodynamics, *Journal of Applied Physics* **104**, 113904 (2008).
- [34] H. Malissa, D. I. Schuster, A. M. Tyryshkin, A. A. Houck, S. A. Lyon, H. Malissa, D. I. Schuster, A. M. Tyryshkin, A. A. Houck, and S. A. Lyon, Superconducting coplanar waveguide resonators for low temperature pulsed electron spin resonance spectroscopy Superconducting coplanar waveguide resonators for low temperature, *Review of Scientific Instruments* **84**, 025116 (2013).
- [35] D. J. Wineland and H. G. Dehmelt, Principles of the stored ion calorimeter, *J. App. Phys.* **46**, 919 (1975).
- [36] S. Gulde, D. Rotter, P. Barton, F. Schmidt-Kaler, R. Blatt, and W. Hogervorst, Simple and efficient photoionization loading of ions for precision ion-trapping experiments, *Applied Physics B: Lasers and Optics* **73**, 861 (2001).
- [37] D. Gerlich, Inhomogeneous RF Fields: A Versatile Tool for the Study of Processes with Slow Ions, *Advances in Chemical Physics* **82** (1992).
- [38] J. D. Prestage, A. Williams, L. Maleki, M. J. Djomehri, and E. Harabetian, Dynamics of charged particles in a Paul radio-frequency quadrupole trap, *Physical Review Letters* **66**, 2964 (1991).
- [39] M. Harlander, R. Lechner, M. Brownnutt, R. Blatt, and W. Hänsel, Trapped-ion antennae for the transmission of quantum information., *Nature* **471**, 200 (2011).
- [40] K. R. Brown, C. Ospelkaus, Y. Colombe, a. C. Wilson, D. Leibfried, and D. J. Wineland, Coupled quantized mechanical oscillators., *Nature* **471**, 196 (2011).
- [41] D. J. Heinzen and D. J. Wineland, Quantum-limited Cooling and Detection of Radio-Frequency Oscillations by Laser-cooled Ions, *Phys. Rev. A* **42**, 2977 (1990).
- [42] N. Daniilidis, T. Lee, R. Clark, S. Narayanan, and H. Häffner, Wiring up trapped ions to study aspects of quantum information, *J. Phys. B* **42**, 154012 (2009).
- [43] J. Eisert, M. B. Plenio, S. Bose, and J. Hartley, Towards quantum entanglement in nanoelectromechanical devices, *Physical Review Letters* **93**, 190402 (2004).
- [44] G. Kurizki, P. Bertet, Y. Kubo, K. Mølmer, D. Petrosyan, P. Rabl, and J. Schmiedmayer, Quantum technologies with hybrid systems, *Proceedings of the National Academy of Sciences of the United States of America* **112**, 3866 (2015).
- [45] N. Leefer, K. Krimmel, W. Bertsche, D. Budker, J. Fajans, R. Folman, H. Häffner, and F. Schmidt-Kaler, Investigation of two-frequency Paul traps for antihydrogen production, *Hyperfine Interactions* **238**, 12 (2016).
- [46] M. Ahmadi, B. X. Alves, C. J. Baker, W. Bertsche, A. Capra, C. Carruth, C. L. Cesar, M. Charlton, S. Cohen, R. Collister, S. Eriksson, A. Evans, N. Evetts, J. Fajans, T. Friesen, M. C. Fujiwara, D. R. Gill, P. Granum, J. S. Hangst, W. N. Hardy, M. E. Hayden, E. D. Hunter, C. A. Isaac, M. A. Johnson, J. M. Jones, S. A. Jones, S. Jonsell, A. Khramov, P. Knapp, L. Kurchaninov, N. Madsen, D. Maxwell, J. T. McKenna, S. Menary, J. M. Michan, T. Momose, J. J. Munich, K. Olchanski, A. Olin, P. Pusa, C. Rasmussen, F. Robicheaux, R. L. Sacramento, M. Sameed, E. Sarid, D. M. Silveira, C. So, D. M. Starko, G. Stutter, T. D. Tharp, R. I. Thompson, D. P. van der Werf, and J. S. Wurtele, Investigation of the fine structure of antihydrogen, *Nature* **578**, 375 (2020).
- [47] M. Brownnutt, M. Kumph, P. Rabl, and R. Blatt, Ion-trap measurements of electric-field noise near surfaces, *Reviews of Modern Physics* **87**, 1419 (2015).